# A parallel plate flow cell for the investigation of the role of surfactants in the codeposition of polymer particles in nickel electroplating

C. FILIATRE*, L. TOWARNICKI, F. MANGE and A. FOISSY
*University of Franche-Comté, Laboratoire d'Electrochimie et des Systèmes Microdispersés, La Bouloie, 25030 Besancon Cédex, France*
(*author for correspondence)

## Abstract

A parallel plate flow cell was designed for the study of particle codeposition in metal electrodeposition. Particle deposition was visualized and recorded with a microscope/video assembly. The effects of two surfactants (anionic sodium dodecyl sulphate and cationic cetyl trimethyl ammonium bromide) on the adhesion of anionic polystyrene particles to a nickel substrate were examined. The deposition rate in laminar flow was measured as a function of the main parameters, that is, electrode potential, Ni(II) concentration, surfactant concentration and pH. The hydrodynamic drag force applies uniformly and tangentially to the collector under laminar flow in contrast with rotating disc or impinging jet cells. No deposition is observed unless specific attractive forces carry the particles through the boundary layer. Particle attachment takes place over a limited range of surfactant/Ni(II) composition and correlates with the formation of a surface film visible under the microscope. Results discussed are based on the adsorption of SDS and CTAB on to both the electrode and the particles, an adsorption which significantly alters the interaction potential at a short distance. The cell gives interesting evidence for the occurrence of specific interactions in electrolytic codeposition. It also proves useful for observing other phenomena, such as hydrogen bubbling.

## 1. Introduction

Composite coatings can be obtained electrolytically by simply adding a micronized powder in the dispersed phase to a regular electrolytic bath. In fact, all kinds of metallic phases (nickel, zinc, cobalt, chromium etc.) and dispersed materials (metal oxides, SiC, organic particles etc.) may be combined to produce composites for innovative or improved surface properties. Thus, a wide scope of applications are possible, such as wear or corrosion resistance, lubrication, adhesion and electrocatalysis. Several review papers [1–3] exist and Fransaer [4] presents a general analysis of interaction forces between approaching particles and metallic surfaces, including electrical and hydrodynamic effects, aiming specifically at the elaboration of electrolytic composites.

The codeposition mechanism can be described in three consecutive steps: (a) transport of particles from the solution to the electrode, (b) adhesion of particles to the substrate, and (c) entrapment of particles in the growing metallic matrix.

The high ionic strength of an electrolytic bath makes electrophoretic migration negligible; the major contribution to particle transport is due to hydrodynamics. The bulk transfer rate of Brownian and micrometric particles has been studied extensively in past years, using different flow rates and interface geometries [5]. The transport of particles in the boundary layer has also been examined, considering both linear adsorption regimes and more complicated situations where perturbations due to previously deposited particles are incorporated into the force fields and the local fluid velocity [6–8]. Many theoretical developments have been confirmed experimentally, using monodisperse latex suspensions and dielectric collectors [6].

The adhesion step is controlled by the particle/surface interaction potential [9], which includes van der Waals and electrical double layer contributions, as described by the well known D.L.V.O. theory [10]. At higher electrolyte concentration, adsorbed solvated species (generally cations) produce strongly repulsive forces [11]. In contrast, attractive interactions may take place between hydrophobic surfaces, or in the presence of adsorbed surfactants [12, 13] or 'bridging' polymers [14]. Additives can affect codeposition in various ways: directly, by adsorption and change of the adhesion properties of either electrode or particles or both, indirectly by modifying the dispersion/aggregation state of the particles. The deaggregation of latex particles in nickel electrolytic baths due to the adsorption of sodium dodecyl sulfate (SDS) and cetyl trimethyl ammonium bromide (CTAB) [15], the dispersion of silicon carbide

(SiC) and silica by poly(vinyl Imidazole) [16] and the decrease in the sedimentation rate by Xanthan gums in nickel/SiC systems [17] illustrate this influence. On the other hand, little is known about the influence of interfacial parameters in the attachment of particles onto the substrate in real electrolytic systems. Attempts were made to relate the electrokinetic (zeta) potential of particles to their codeposition properties, but these were necessarily limited to dilute solutions [18].

The third step involves a complex superposition of chemical and electrical interactions: desorption of the solvent and other bound molecules and ions, neutralization of the particle surface charge, transfer of electronic charge, and growing of the metallic matrix around embedded particles. Until now, these phenomena were essentially examined through the particle induced alterations in polarization curves and current efficiencies [19]. More recent studies, involving electron microscopy, electrochemical impedance and noise measurements, coupled with well controlled hydrodynamics, have opened up new vistas for kinetic investigations of particle collisions and codeposition reactions [20].

The present work describes a cell specifically designed for investigating electroadhesion. The relevance of the cell in codeposition studies is exemplified by analysing the effect of surfactants in a polystyrene particle/nickel electrolytic bath. For this purpose, cationic (CTAB) and anionic (SDS) surfactants were used, since both were shown earlier to assist, or strongly alter, codeposition [15, 18].

## 2. Parallel flow cell

### 2.1. Parallel cell versus other geometries

The parallel plate flow cell does not a priori favour the deposition yield compared to the rotating disc electrode (RDE), or the impinging jet cell (IJC) where the stagnation point flow brings the particle to the electrode [5]. In a parallel flow cell, the particle flux perpendicular to the electrode relies on the existence of an external force, for instance, electrophoresis, sedimentation or specific attractive forces close to the substrate. In a plating solution no contribution to particle transport is expected from electrophoretic migration. Thus only specific forces may operate.

In addition the fluid flow exerts lifting [21] and tangential shearing forces that tend to reduce the deposition rate. It has been shown that the lifting force, which is due to velocity gradients across the particle diameter can be neglected at low Reynolds numbers [4, 22]. In contrast, one expects a large effect of the tangential force in the removal of particles that happen to adsorb onto the surface [23]. For a spherical particle, this force is expressed by,

$$Ft = 15.3 \, Pmr(1 - ((b - r)/b)^2)Q/S \tag{1}$$

where $m$, $r$, $Q$ are, respectively, the viscosity, the particle radius and the flow rate, $b$ is the half distance between the plates and $S$ is the area of the cross section of the cell [24].

### 2.2. Description of the cell

The cell allowed *in situ* observations of hydrodynamic and adhesion/detachment phenomena. A schematic representation of the cell from a top view is given in Figure 1. The liquid flows in a rectangular channel, between two parallel PMMA plates assembled tightly through an o-ring. The top of the figure shows the removable cathodic plug comprising a circular metallic electrode (1 cm$^2$ nickel foil in the present work). The PMMA plate at the bottom contained the conductive glass (coated with a tin oxide film) acting both as a window and a counter electrode. Both electrodes were connected to the power supply (EG&G). A silver wire, inserted through the plug, served as a pseudoreference. The channel were 2 mm thick (between facing electrodes), 20 mm wide (perpendicular to the plane of the figure) and 200 mm long, thus ensuring fully developed laminar flow at the location of the electrodes in the cell [24].

For all experiments the longer cell dimension was above the horizontal axis. The electrodes and the wide side of the rectangular channel were positioned vertically. The optical and measurement setup contained a ×20 long working distance objective, allowing observation of 1 to 100 $\mu$m particles between the two facing electrodes, a microscope (Olympus), a video recorder (Sony) and an image analysing system (Aries, Esilab). The observed area was 0.11 mm$^2$. The entire setup is summarised in Figure 2.

Steady flow was maintained by gravity between two reservoirs placed on each side of the cell. A peristaltic pump allowed recycling to maintain constant liquid levels. The flow rate was measured by weighing and timing a sample of flowing solution. Under typical working conditions the flow was laminar. Certification was made by measuring the velocity profile of polystyrene
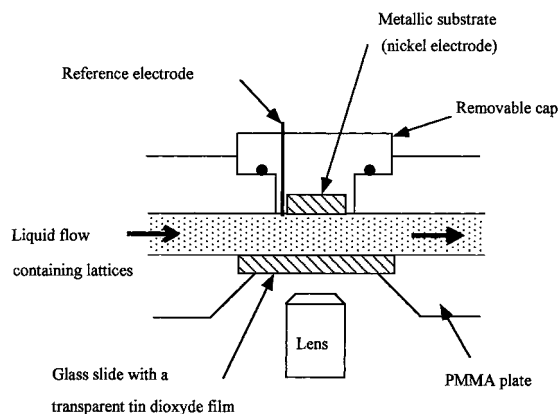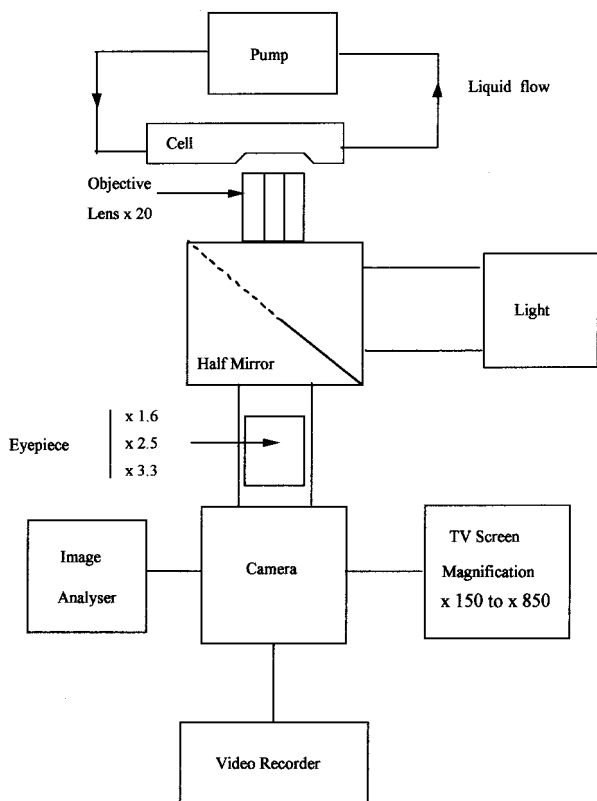


*Fig. 1.* Top view of the cell.

Fig. 2. Schematic view of the experimental set-up.

particles (4 $\mu$m in diameter), in the absence of an applied field, using several stream rates up to 0.07 cm$^3$ s$^{-1}$. The last value corresponds to a Reynolds number of about one. As an example, Figure 3 shows the expected parabolic velocity profiles at flow rates of 0.02 and 0.06 cm$^3$ s$^{-1}$.
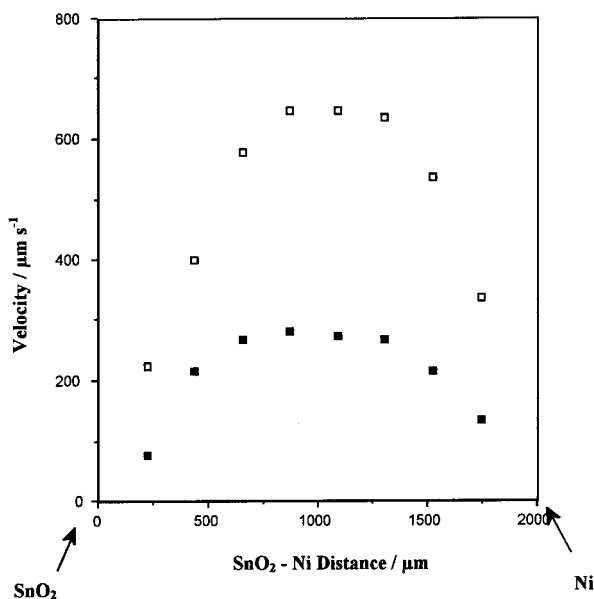


Fig. 3. Fluid velocity profiles in the cell liquid flows: 0.02 cm$^3$ s$^{-1}$ ($\blacksquare$); 0.06 cm$^3$ s$^{-1}$ ($\square$).

## 3. Materials

### 3.1. Preparation and size distribution of polystyrene particles

Polystyrene (PS) particles were prepared at the Laboratoire de Chimie et des Procédés de Polymérisation (LCPP, CNRS, Villeurbanne, France) using emulsion polymerization with persulfate salts as an initiator. PS particles were further purified by a mixture of cationic and anionic exchange beds, followed by an exhaustive dialysis using a large volume of high resistivity water, in order to remove salt and surfactant residues up to a conductivity of 2 mS cm$^{-1}$. The PS particle average diameter determined by electron microscopy was 4 $\mu$m.

### 3.2. Adsorption measurements

Adsorption of surfactants on the PS particles was calculated by the difference between the total amount introduced and that remaining in the solution after separation of the PS particles by centrifugation. Organic carbon analysis (TOC-5050, Shimadzu) was used for titrating surfactants in the solution.

### 3.3. Surface properties of polystyrene particles

Electrophoretic mobility illustrates the surface properties of the PS particles and their dependence on the cationic (CTAB) and anionic (SDS) surfactants, combined with nickel ions. Detailed analysis of the ionization and adsorption properties of the polystyrene particles may be found elsewhere [15].

After dialysis, the PS particle dispersion was diluted to 1 wt% and sonicated. Electrophoretic mobilities were measured with a Mark II apparatus (Rank Brothers, Bottisham) using particles diluted in their own supernatant. The electrical charge on the PS particles originates mainly from the ionization of sulphate formed by the polymerization initiators and possibly by anchored surfactant molecules (sodium dodecyl sulphate) introduced during the emulsification step. The nature and density of surface chemical groups were determined using pH and conductometric titrations [15]. PS particles have a sulphate group density on the surface close to 0.22 nm$^{-2}$, corresponding to a surface charge of $3.6 \times 10^{-2}$ C m$^{-2}$. In the present aqueous medium, PS particles, being highly hydrophobic, tend to aggregate.

Owing to their strong acidic sulphate groups, PS particles exhibit a negative charge with a mobility of about $-2 \times 10^{-8}$ m$^2$ V$^{-1}$ s$^{-1}$ (Figure 4). In the presence of nickel ions, the electrophoretic mobility of PS particles decreases considerably (Figure 4) and SDS does adsorb, as shown Figure 5 with the isotherms drawn at pH 4, room temperature. The nickel induced adsorption is due to electrostatic bridging between particles (sulfate groups) and SDS molecules or micelles [15]. At an SDS concentration of $5 \times 10^{-4}$ M, adsorption
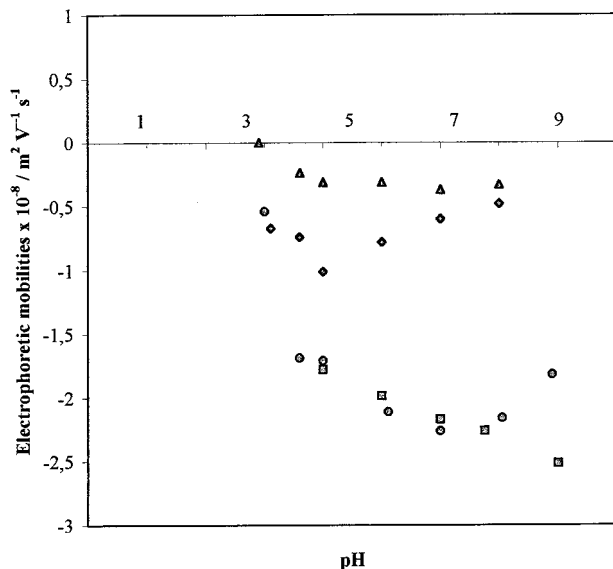
Fig. 4. Electrophoretic mobilities of PS lattices against pH: aqueous solution (□); $10^{-3}$ M Ni(II) (△); $5 \times 10^{-4}$ M SDS (◉); $10^{-3}$ M Ni(II) + $10^{-4}$ M SDS ( ).

is only one third of full coverage, which is confirmed by the absence of significant modification of electrophoretic mobility (Figure 4). At an SDS concentration of $5 \times 10^{-3}$ M, adsorption reaches 2.5 molecules nm$^{-2}$, which corresponds to the saturation of the surface. At saturation level, SDS molecules do not form a homogeneous bilayer on the PS particle, which would give a density of about 4 nm$^{-2}$. Molecules more likely bind tails onto the hydrophobic part of the surface (heads toward the solution) and form micelles or hemi-micelles on the sulfate groups.

In comparison with the preceding values obtained in solutions containing Ni(II) at the concentration of $10^{-2}$ M, adsorbed quantities are lower in $10^{-3}$ M nickel solution and higher in a regular Watts bath (Ni(II) 1.2 M)
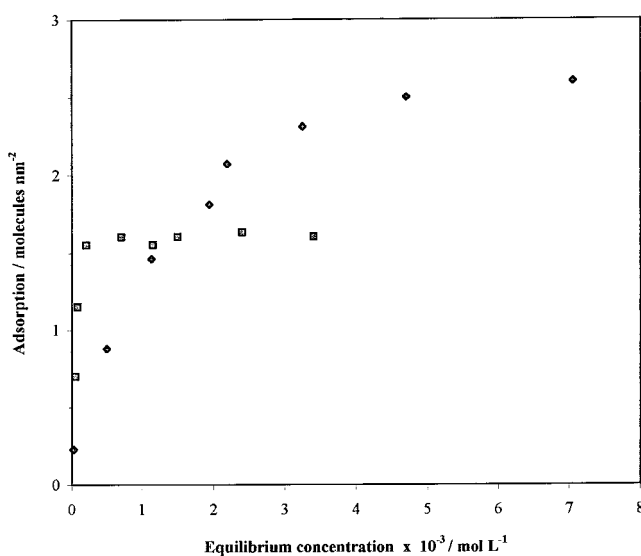
[15]. In the presence of both nickel ions ($10^{-3}$ M) and SDS ($10^{-4}$ M), PS particles remain slightly negative, with a mobility of about $-1 \times 10^{-8}$ m$^2$ V$^{-1}$ s$^{-1}$ (Figure 4).

Addition of the cationic CTAB produces a reversal of charge of the PS particles in a dilute Watts solution (Nickel $10^{-3}$ M, pH 4) (see Figure 6). In comparison with SDS, CTAB strongly adsorbs onto the PS particles (Figure 5). At the onset of the adsorption plateau, the equilibrium concentration of CTAB in the solution is below $5 \times 10^{-4}$ M, instead of $5 \times 10^{-3}$ M with SDS.

## 4. Deposition measurements

### 4.1. Experimental procedure

A Watts-type nickel electrolytic bath was used (called below the 'basic solution') containing NiSO$_4$.6H$_2$O (1.05 M), NiCl$_2$.6H$_2$O (0.15 M) and H$_3$BO$_3$ (0.65 M).

The electrode potential was incremented between 0 and $-2$ V (vs Ag wire) in steps of 0.1 V. For each step the current was monitored and the potential difference was maintained for 3 min after the current had been stabilized. If no latex deposition was observed, the potential was increased. The experiment was stopped when hydrogen bubbles formed at the electrode. The maximum current density was about 10 A m$^{-2}$. When no specific mention is made, the flow rate was 0.05 cm$^3$ s$^{-1}$. All potential measurements of the collecting electrode refer to the silver wire immersed in the solution. Separate measurements of the potential difference between the silver calomel electrode gave $+19$ mV and $+150$ mV in the basic and in the dilute nickel solutions, respectively.

Deposition experiments were carried out using the basic or the $10^3$ times dilute nickel bath, to which SDS or CTAB surfactants were added. The various experiments are summarized in Table 1.
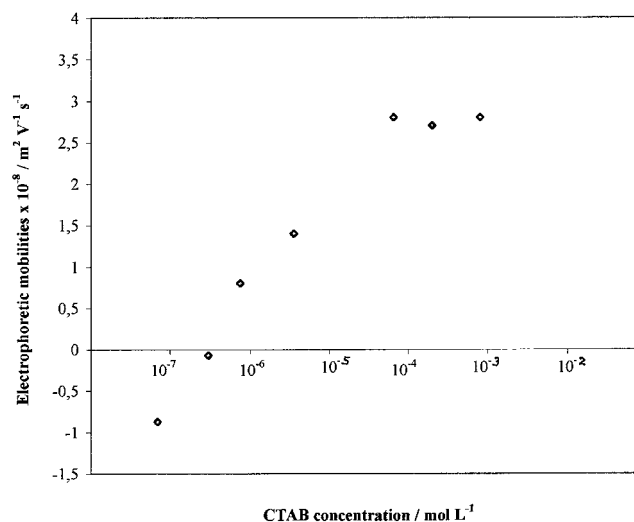


Fig. 5. Surfactant adsorption isotherm on PS lattices, pH 4, $10^{-2}$ M Ni(II) SDS ( ), CTAB (□).



Fig. 6. Electrophoretic mobilities of lattices versus CTAB concentration (M), $10^{-2}$ M NiSO$_4$, pH 4.

*Table 1.* Summary of experiments at various concentrations of nickel and surfactants

| Nickel concentration /M | SDS concentration /M | CTAB concentration /M | Particle deposition |
|---|---|---|---|
| 0 | 0 | 0 | no |
| $10^{-3}$ | 0 | 0 | no |
| 1,2 | 0 | 0 | no |
| 0 | $5 \times 10^{-4}$ | 0 | no |
| $10^{-3}$ | $5 \times 10^{-5}$ | 0 | yes |
| $10^{-3}$ | $5 \times 10^{-4}$ | 0 | yes |
| $10^{-3}$ | $5 \times 10^{-3}$ | 0 | no |
| 0 | 0 | $5 \times 10^{-4}$ | no |
| $10^{-3}$ | 0 | $5 \times 10^{-5}$ | yes (aggregates) |
| $10^{-3}$ | 0 | $5 \times 10^{-4}$ | yes |
| $10^{-3}$ | 0 | $5 \times 10^{-3}$ | yes |

### 4.2. *Deposition in the basic nickel bath*

To determine the relative magnitude of hydrodynamic and electrophoretic forces, observations were made concerning PS particles in the cell, as a function of potential applied, in systems containing various amounts of nickel ions. The pH value of the solution was 4 in each case (pH was adjusted using a solution of hydrochloric acid). In the absence of nickel ions, the flow of PS particles was not altered by the electric field from 0 to $-1$ V (vs silver wire). At more negative potentials of the collecting electrode (cathode), PS particles move away from the cathode but do not cross the cell because at some point the liquid flow carries them along.

At a nickel concentration of $10^{-3}$ M, PS particles migrate to the anode between $-1.0$ V and $-1.7$ V, but migration starts to reverse to the cathode at a potential of $-1.7$ V. At this potential PS particles slow down, roll over the electrode, without any deposition taking place. At higher (cathodic) potentials, bubbles are formed on the substrate, hampering PS particle deposition.

In a regular Watts bath (Ni(II) 1.2 M), PS particles do not deviate from the fluid flow up to the electrode potential $-1.7$ V. At this point they also move to the cathode and behave as above.

These experiments indicate that the balance between longitudinal forces (hydrodynamic) and transversal forces (electrophoretic, diffusional etc.) is very sensitive to bath composition and operational parameters.

### 4.3. *Influence of surfactant addition*

The influence of surfactant addition was investigated at three concentrations: $5 \times 10^{-5}$, $5 \times 10^{-4}$ and $5 \times 10^{-3}$ M in the same nickel solutions as above.

#### 4.3.1. *Anionic surfactant (SDS)*
The deposition behaviour of PS particles is not altered by adding SDS ($5 \times 10^{-4}$ M) in the absence of nickel ions. This is consistent with the fact that SDS does not adsorb and therefore does not modify the surface properties.

In a dilute Watts bath (Ni(II) $10^{-3}$ M), PS particle deposition depends on SDS concentration and substrate polarization. At lower SDS concentration ($5 \times 10^{-5}$ M), PS particles start to deposit at $-1.7$ V. At this potential, deposition increases with SDS concentration, peaks at about $5 \times 10^{-4}$ M and disappears at $5 \times 10^{-3}$ M.

In general, smaller PS particles deposit preferentially to larger ones. Practically, small PS particles reach the electrode at $-1.5$ V. They also wander less over the substrate than larger ones. This is in qualitative agreement with Equation 1, where the hydrodynamic force is shown to increase linearly with particle size.

One of the curves in Figure 7 shows the deposition rate as a function of time at an SDS concentration of $5 \times 10^{-4}$ M. After the experiment, the electrode is removed and dried in air. A white film appears on the substrate, with deposited PS particles entrapped inside (Figure 8).

SDS does not induce any PS particle deposition in a regular electrolytic bath (Ni(II) 1.2 M). At a potential of $-1.5$ V, PS particles start to migrate towards the cathode, but they slide upwards. This may be attributed to the effect of a large difference in specific weight between the particles and the solution near the interface, or to some hydrodynamic instability due to ionic migrations and pressure gradients at the onset of nickel deposition [7, 8].

#### 4.3.2. *Cationic surfactant (CTAB)*
In the presence of CTAB (concentrations $5 \times 10^{-5}$, $5 \times 10^{-4}$ and $5 \times 10^{-3}$ M) and nickel concentration $10^{-3}$ M, PS particles no longer move away from the cathode. Deposition starts at the electrode potential of $-1.5$ V for the three surfactant concentrations, but hydrogen bubbles strongly disturb the flow of particles. Differences between the three CTAB concentrations appear in the aspect of deposited units: aggregates at a concentration of $5 \times 10^{-5}$ M and uniformly distributed primary particles at $5 \times 10^{-4}$ M.

As shown in Figure 7, deposition rates are very similar in CTAB and SDS solutions over a short period. After an experimental time, above some 70 to 100 min, deposition rates reach a plateau. At the plateau, the surface coverage is about 9000 particles per mm$^2$ with SDS and 13 500 with CTAB. These values correspond roughly to a coverage ratio of 15% and 20%, respectively, which is in good agreement with other experiments and theoretical predictions presented by Adamczyck et al. [5]. The decrease in the deposition rate (rounding of the deposition-time curve) and the saturation plateau values, much below 100% coverage, are explained by a strong 'shadow effect' induced by already deposited particles. Practically, when particles do not attract each other, formerly deposited particles force incoming ones away from the substrate [4, 5].

### 4.4. *Influence of pH and flow rate*

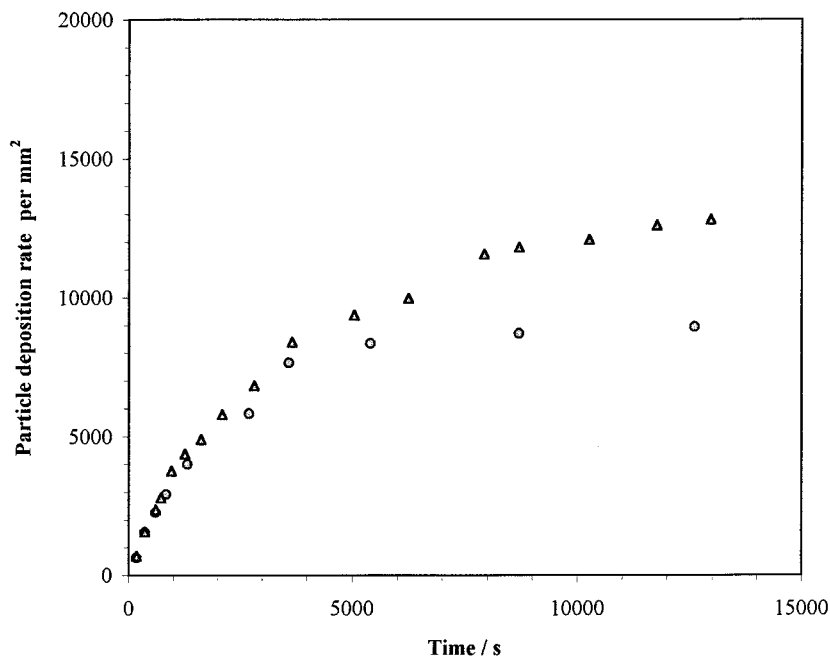Figure 9 shows the deposition yield at various pH and flow rates. Time was taken as zero at the electrode

*Fig. 7.* Deposition yield of PS lattices up to the saturation level, pH 4, electrode surface 0.1 mm$^2$, surfactant concentration $5 \times 10^{-4}$ M, SDS solutions (◎), CTAB solutions (▦).

potential $-1.7$ V. Deposition rate values at time zero correspond, therefore, to particles attached during the stepwise increase in potential. As expected qualitatively from the increase in the tangential hydrodynamic force (Relation 1), the deposition rate decreases as the flow rate increases. At high flow rates (0.05 and 0.14 cm$^3$ s$^{-1}$), the deposition rate increases linearly with deposition time for the first 600 s and does so for a shorter time at the lower flow rate (0.01 cm$^3$ s$^{-1}$). The rounding in the deposition curve, as a result of the shadow effect of formerly-deposited particles, takes place sooner at higher deposition rates.

At a flow rate of 0.05 cm$^3$ s$^{-1}$, the deposition rate decreases between pH 5.7 and pH 3.6. Because there is

no change in the electrophoretic mobility and SDS adsorption properties of PS particles between these two pHs, the decrease in the deposition rate with decrease in pH is possibly caused by the observed higher rate of release of hydrogen bubbles.

## 5. Discussion

Conditions favourable to spontaneous adhesion have been found for a limited range of surfactant and Ni(II) concentrations, but no deposition was observed in dispersions containing only one of these two components. In addition, no deposition was obtained in a regular electrolytic bath. To explain the results, two kinds of phenomena will be considered, those relating to particle/solution interface and particle/electrode interactions.

In a dilute Watts bath, the particles are negatively charged (Figure 4) and migrate to the anode. At the potential where the reduction of nickel ions starts (about $-1.5$ V), particles migrate towards the cathode, but no attractive force brings the particles a state of permanent attachment with the electrode. The main difference between dilute and basic Watts solutions is, in the latter case, that no anodic migration takes place between $-1$ and $-1.7$ V. This is explained by a decrease in the electric field, as a consequence of the corresponding increase in bath conductivity.

PS particles do not deposit when SDS is added in the absence of nickel ions. We may refer to detailed studies of the mercury/SDS solution interface [12, 25]. Using electrocapillary curves and impedance spectroscopy, the authors report the formation of stable SDS adsorption
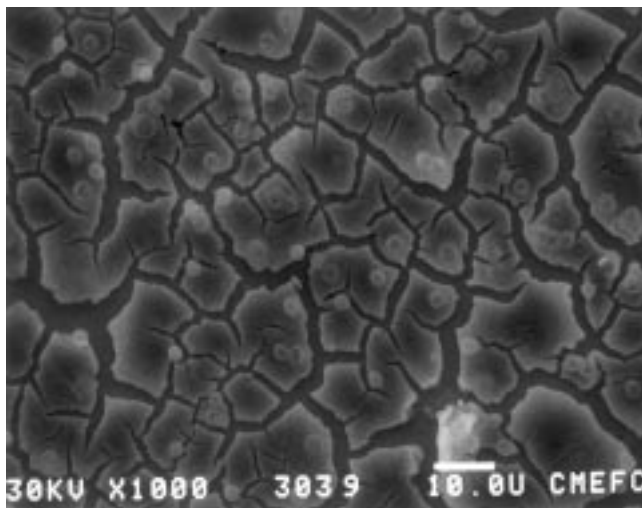


*Fig. 8.* Dried film containing particles. Experimental conditions: $10^{-3}$ M Ni(II), $5 \times 10^{-4}$ M SDS, pH 4.
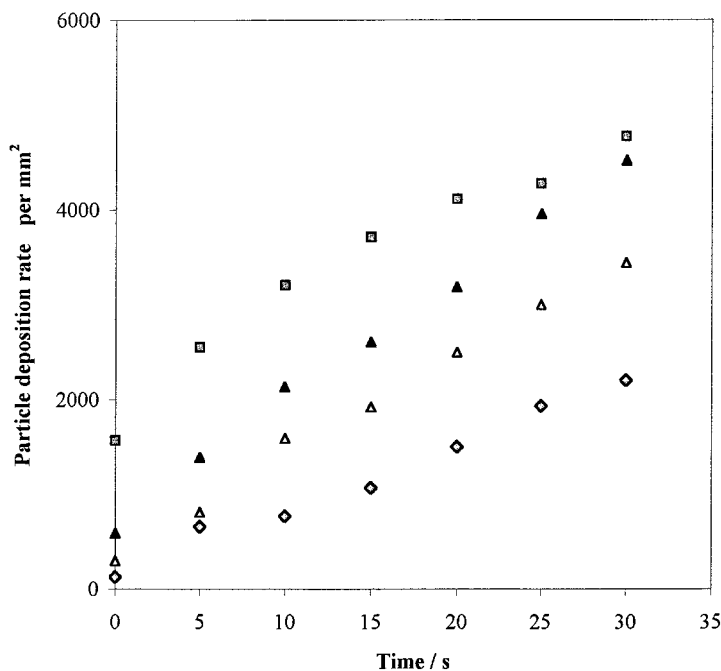
*Fig. 9.* Particle deposition yield in $10^{-3}$ M Ni(II), $5 \times 10^{-4}$ M SDS solutions at different flow rates and pH: 0.01 cm$^3$ s$^{-1}$, pH 5.7 (▣); 0.05 cm$^3$ s$^{-1}$, pH 5.7 (▲); 0.14 cm$^3$ s$^{-1}$, pH 5.7 ( ); 0.05 cm$^3$ s$^{-1}$, pH 3.6 (△).

layers containing up to 1.7 mol nm$^{-2}$ at a concentration of $5 \times 10^{-4}$ M. It is interesting to note that the adsorption of negative SDS molecules takes place up to polarization potentials of 500 mV more cathodic than the potential of zero surface charge. These data demonstrate the strong affinity of SDS molecules for the metallic surface. SDS adsorb through hydrophobic bonds between the electrode and the aliphatic tail, pointing negative functional groups towards the solution [12]. Assuming that SDS behaves similarly on nickel and mercury electrodes, due to SDS adsorption on the substrate, a strong electrostatic barrier prevents negative PS particles from depositing in solutions containing no nickel ions.

In the presence of nickel ions, both the electrode and the particles have different affinities for SDS. At the lower surfactant concentration ($5 \times 10^{-5}$ M), SDS covers the electrode surface but does not adsorb onto the PS particles. At an SDS concentration of $5 \times 10^{-4}$ M, adsorption is about 30% of a monolayer on the PS particles and at a concentration of $5 \times 10^{-3}$ M, it forms a saturated monolayer (Figure 5). Nickel ions influence particle/electrode interaction forces and, as a result, the deposition rates of PS particles. At a lower SDS concentration, particle deposition in $10^{-3}$ M nickel solutions is explained by the reduction in the electrostatic barrier caused by the screening effect of nickel ions. Once the particles have penetrated through the SDS layer, attachment to the electrode is made possible by means of hydrophobic bonds between the PS particle surface and the SDS tails. At an SDS concentration of $5 \times 10^{-4}$ M the particles remain sufficiently hydrophobic but at a concentration of $5 \times 10^{-3}$ M, since SDS covers completely the surface, there is no longer a hydrophobic

bond to stabilize the PS particles in the surfactant layer and deposition returns to zero. Direct measurements of interaction forces support the above explanation. Data were produced for the disjoining pressure [26] between a mercury electrode and gas bubbles (air or nitrogen) in SDS solutions containing $10^{-4}$ M NaClO$_4$ [13]. The authors report spontaneous attachment between mercury and gas bubbles for SDS concentrations up to $5 \times 10^{-6}$ M. Calculation of the mercury/bubble interaction potential leads the authors to conclude that an attractive hydrophobic force balances the repulsive van der Waals and electrostatic forces. In the present study, the mercury/bubble interface is replaced by one between nickel and PS particles. Although differences exist (PS particles carry a low negative charge, presence and electrolysis of nickel ions, range of polarization potential) the phenomena appear qualitatively similar in terms of SDS concentration dependence.

In contrast to SDS, CTAB adsorbs on to a negative electrode with the positive group on the metal and the cetyl tail towards the solution, giving the cathode hydrophobic properties [12]. At higher surfactant concentrations, a second layer is formed on the electrode, with positive head groups toward the solution. The absence of deposition in pure CTAB solutions ($5 \times 10^{-4}$ M) is thus explained by the electrostatic repulsion between adsorbed surfactant layers on the electrode and on the positive PS particles. For CTAB in dilute nickel solutions, deposition occurs at all surfactant concentrations between $5 \times 10^{-5}$ and $5 \times 10^{-3}$ M. At CTAB concentration of $5 \times 10^{-5}$ M aggregate deposition is observed. At this concentration, adsorption of CTAB is just sufficient to neutralize the PS surface charge (Figure 5) allowing aggregation to take place through

hydrophobic attraction forces. At higher CTAB concentrations ($5 \times 10^{-4}$ and $5 \times 10^{-3}$ M), adsorption of CTAB reaches full coverage (Figures 5 and 6), producing positive particles that no longer aggregate due to sufficient electrostatic repulsion. In these conditions, experiment shows that stabilization against aggregation does not prevent PS particle deposition. The latter is associated, as it is in all cases, with the formation of an apparent film at the electrode, again showing the occurrence of a specific electrochemical entrapment. The chemical nature of the film has not been elucidated. It probably consist of some hydrolysed nickel species.

## 6. Conclusions

The electrolysis cell described in this paper has proved to be useful for the study of codeposition of particles in composite plating. We observed that negatively charged polystyrene particles adsorb on to the negative electrode, under the condition that nickel ions and surfactants such as SDS, CTAB, Poly(acrylic acid) (unpublished result) are present in the bath.

Surfactants directly influence electroadhesion by modifying the interfacial properties of both the particles and the electrode. By preventing the aggregation of particles in the bath, they may also enhance particle deposition.

Nickel ions act as charge reducers in two ways: they promote SDS adsorption on to the particles and they screen the electrostatic repulsion forces between surfactant layers at the electrode surface. There is some evidence that nickel ions and surfactant participate in the formation of an optically detectable film in a limited range of potential values and salt and surfactant concentrations. The film occurrence, apparently correlates with PS particle deposition.

In the present experiment, the measurements were made at 25 °C instead of the temperature currently used in nickel electrodeposition (i.e., about 50 °C). Further investigations are necessary in order to establish correlations between interfacial phenomena and deposits in industrial codeposition systems.

## References

1. J.P. Celis, J.R. Roos, C. Buelens and Y. Fransaer, *Trans. Inst. Met. Finish.* **69** (1991) 133.
2. J. Fransaer, J.P. Celis and J.R. Roos, *Metal Finish.* **91** (1993) 97.
3. A. Hovestad and L.J.J. Janssen, *J. Appl. Electrochem.* **25** (1995) 519.
4. J. Fransaer, PhD thesis (Katholieke Universiteit Leuven, 1994).
5. Z. Adamczyk, B. Siwek, M. Zembala and P. Belouschek, *Adv. Colloid Interface Sci.* **48** (1994) 151.
6. Z. Adamczyk and P. Warszynski, *Adv. Colloid Interface Sci.* **63** (1996) 41.
7. M. Trau, D.A. Saville, I.A. Aksay, *Science* **272** (1996) 706.
8. S. Yeh, M. Seul and B.I. Shralman, *Nature* **386** (1997) 57.
9. J. Israelachvilli, 'Intermolecular and Surface Forces', 2nd edn (Academic Press, London, 1992).
10. B. Derjaguin, *Kolloid Z.* **69** (1934) 55.
11. R.M. Pashley, *J. Colloid Interface Sci.* **83** (1981) 531.
12. M. Kaisheva, S. Usui and Dai Qi, *Colloids Surfaces* **29** (1988) 147.
13. Q. Day, H. Sasaki, S. Usui and M. Keisheva, *J. Colloid Interface Sci.* **139** (1990) 30.
14. M.L. Janex, V. Chaplain, J.L. Counord, R. Audebert, *Colloid Polymer Sci.* **275** (1997) 352.
15. F. Mange, PhD thesis (Université de Franche-Comté, Besançon, 1996).
16. B. Cabot, A. Deratani and A. Foissy, submitted to *Colloids and Surfaces* (1998).
17. N. Desbois, PhD thesis (Université de Franche-Comté, Besançon, 1992).
18. T. Hayashi, N. Maeda and N. Furukawa, *Opperviaktechnieken* **10** (1978) 246.
19. P.R. Webb and N.L. Robertson, *J. Electrochemical Soc.* **141**(3) (1994) 669.
20. V. Bouet, J. Fransaer, F. Huet, G. Maurin and J.P. Celis, *J. Electrochem. Soc.* **145**(2) (1988) 436.
21. P.G. Saffman, *J. Fluid Mech.* **22** (1965) 385.
22. M.L. Janex, PhD thesis (Université de Paris VI, 1994).
23. M.M. Sharma, H. Chamoun, D.S.H. Sita Rama Sarma and R.S. Schechter, *J. Colloids Interface Sci.* **149**(1) (1992) 121.
24. E. Guyon, J.P. Hulin and L. Petit, 'Hydrodynamique Physique' (Intereditions/Editions du CNRS, Paris et Meudon, 1991).
25. M. Kaisheva, *Adv. Colloids Interface Sci.* **38** (1992) 319.
26. A.W. Adamson, 'Physical Chemistry of Surfaces', 3rd edn. (Wiley, New York and London, 1976).